

Gamma Ray and Neutrino Flux from Annihilation of Neutralino Dark Matter at Galactic Halo Region in mAMSB Model

Kamakshya Prasad Modak¹ and Debasish Majumdar²

*Astroparticle Physics and Cosmology Division,
Saha Institute of Nuclear Physics,
1/AF Bidhannagar, Kolkata 700064, India.*

Abstract

We consider the lightest supersymmetric particle (LSP), neutralino in minimal anomaly mediated supersymmetry breaking model (mAMSB) to be a possible candidate for weakly interacting massive particles (WIMP) or cold dark matter and investigate its direct and indirect detections. The theoretically allowed supersymmetric parametric space for such a model along with the recent bounds from LHC is constrained by the WMAP results for relic densities. The spin independent and spin dependent scattering cross sections for dark matter off nucleon are thus constrained from the WMAP results. They are found to be within the allowed regions of different ongoing direct detection experiments. The annihilation of such dark matter candidates at the galactic centre produce different standard model particles such as gamma rays, neutrinos etc. In this work, we calculate the possible fluxes of these γ -rays and neutrinos coming from the direction of the galactic centre (and its neighbourhood) at terrestrial or satellite borne detectors. The calculated γ -ray flux is compared with the observational results of HESS experiment. The neutrino flux of different flavours from the galactic centre and at different locations away from the galactic centre produced by WIMP annihilation in this model are also obtained for four types of galactic dark matter halo profiles. The detection prospects of such ν_μ coming from the direction of the galactic centre at the ANTARES under sea detector are discussed in terms of muon signal yield from these muon neutrinos. Both the gamma and neutrino signals are estimated for four different dark matter halo profiles.

¹email: kamakshya.modak@saha.ac.in

²email: debasish.majumdar@saha.ac.in

1 Introduction

Cosmological observations like flattening of rotation curves of spiral galaxies [1], the gravitational microlensing [2], observations on Virgo and Coma clusters [3, 4], bullet clusters [5], etc. provide indications of existence of huge amount of non-luminous matter or dark matter (DM) in the universe. The Wilkinson Microwave Anisotropy Probe (WMAP) experiment [6] suggests that more than 80% of the total matter content of the universe (almost 23% of the total content of the universe) is dark matter. The general wisdom is that in order to account for the relic abundance of DM, a candidate for dark matter should be massive, very weakly interacting and non-relativistic (cold dark matter or CDM) particles. This allows the structure formation on large scales. In the present work, we consider such weakly interacting massive particles (WIMPs) [7, 8, 9, 10] to consist of the total DM content of the universe.

Because of its nature, the detection of dark matter is very challenging experimental effort. In general there are two types of detection mechanism namely direct detection of dark matter and indirect detection of dark matter. The indirect detection of dark matter involves detecting the particles (and their subsequent decays) or photons produced due to dark matter annihilations. These annihilation products can be fermions or γ photons. The dark matter particles, if trapped by the gravity of a massive body like sun or galactic centre, can annihilate there to produce these particles. Study of such photons and fermions such as neutrinos thus throw light on the nature of galactic dark matter as well as the nature of the galactic dark matter halo profile. Different satellite-borne and ground-based experiments looking for extra terrestrial gamma signals have reported the observance of excess gamma ray signals in the direction of galactic centre in different energy regions. If the observed TeV gamma rays from the galactic centre are indeed due to the annihilation of dark matter at galactic centre then such dark matter mass should be \sim TeV. The HESS (The High Energy Stereoscopic System) [11, 12] experiment had reported the gamma rays from the galactic centre with energies in TeV range. In minimal anomaly mediated supersymmetry breaking (mAMSB) model [13, 14], the lightest supersymmetric particle (LSP) neutralino that can be a candidate for dark matter has its mass in TeV range. The calculated γ -ray flux is found to be within the experimental search limit of high energy gamma ray search experiments such as HESS.

The dark matter candidate in the present work is considered to be the lightest supersymmetric particle (LSP) neutralino in the minimal anomaly mediated supersymmetry breaking model where the LSP is stabilised by conservation of R-parity. In the superconformal Anomaly Mediated Supersymmetry Breaking (AMSB) mechanism, dynamical or spontaneous breaking is supposed to take place in some ‘hidden’ sector (HS) and this breaking is mediated to the observable sector (OS) by gravitino

mass ($m_{\frac{3}{2}} \sim 100$ TeV). Supersymmetry breaking effects in the observable sector have a gravitational origin in this framework. In ordinary gravity-mediated supersymmetry breaking model, the supersymmetry breaking is transmitted from HS to OS via tree level exchanges with gravitational coupling. But in AMSB, the HS and the OS superfields are assumed to be located in two parallel but distinct 3-branes and the 3-branes are separated by bulk distance which is of the order of compactification radius, r_c . Thus any tree level exchange with mass higher than the inverse of r_c is exponentially suppressed. So, the supersymmetry breaking is propagated from the HS to the OS via loop generated superconformal anomaly.

In AMSB model, the slepton mass-squared terms are negative giving to tachyonic states. The problem is circumvented by adding an universal mass-squared term m_0^2 to all the squared scalar masses in the minimal extension to this theory, namely, minimal anomaly mediated supersymmetry breaking (mAMSB) model [13, 14]. A sparticle spectrum in this model is fixed by three parameters, $m_{\frac{3}{2}}$ which is gravitino mass, $\tan\beta$ which is the ratio of the vacuum expectation values of the two Higgs fields (H_1^0 and H_2^0) and $\text{sign}(\mu)$, where μ is the Higgsino mass. Thus four parameters are needed to generate spectrum in mAMSB. The neutralino is the lowest mass eigenstate of linear superposition of photino ($\tilde{\gamma}$), zino (\tilde{Z}), and the two Higgsino states (\tilde{H}_1^0 and \tilde{H}_2^0) [15], written as,

$$\chi = a_1\tilde{\gamma} + a_2\tilde{Z} + a_3\tilde{H}_1^0 + a_4\tilde{H}_2^0 . \quad (1)$$

in the basis $\begin{pmatrix} \tilde{\gamma} & \tilde{Z} & \tilde{H}_1^0 & \tilde{H}_2^0 \end{pmatrix}$.

The ATLAS collaboration [16] has recently performed an improved analysis and give a new constraint on the chargino mass to ~ 118 GeV. This new constraint differs from the previous LEP2 bound. In this work, the SUSY parameter space namely m_0 , $m_{\frac{3}{2}}$, $\tan\beta$ and $\text{sign}(\mu)$ is initially adopted from Datta *et al.* [17] but with proper incorporation of the recent LHC (ATLAS) bound on chargino mass [16] mentioned above. The relic densities for such dark matter are then computed using these SUSY parameters and they are compared with the WMAP results. The parameters, thus constrained further by the WMAP results, are then used to calculate the spin independent and spin dependent cross sections (σ_{scatt}) for different neutralino masses (m_χ) (obtained using the restricted parameter space). The χ -nucleon scattering process is essential for the direct searches of dark matter. As mentioned above, we calculate χ -nucleon elastic scattering cross section σ_{scatt} for the restricted parameter space discussed earlier. The $m_\chi - \sigma_{\text{scatt}}$ region, thus obtained, is found to be within the allowed limits of most of the direct detection experiment results.

Using the constrained mAMSB parameter space discussed above we calculate the gamma ray flux in the direction of the galactic centre. These studies are performed for different galactic dark matter halo profiles. We find that the gamma spectrum from galactic centre and halo produced by neutralino dark matter within the frame-

work of the present mAMSB model, is highly energetic. The experiment like HESS, that can probe high energy gamma rays and which, being in the southern hemisphere has better visibility of the galactic centre, will be suitable to test the viability of the present dark matter candidate in mAMSB model. The possibility of detecting neutrinos from galactic centre and halo from dark matter annihilations are also addressed with reference to ANTARES (Astronomy with a Neutrino Telescope and Abyss environmental RESearch) [18] under sea neutrino experiment.

In a recent work Vásquez *et al.* [19] has given a detailed analysis of the allowed parameter space for a neutralino dark matter in the framework of NMSSM model. In their case the dark matter (neutralino) mass was within the range of ~ 80 GeV and hence the energies of the gamma rays from such dark matter annihilations can be probed by FermiLAT [20] experiment. In the present calculation, we instead consider the neutralino dark matter in mAMSB model mentioned above. Some of the earlier works on dark matter phenomenology in AMSB model include Baer *et al.* [21], Moroi *et al.* [22], Ullio [23] etc. In Refs. [21] and [23] the γ flux from the galactic centre are discussed and although neutrinos from the neutralino annihilations are mentioned in Ref. [21] but they have not discussed elaborately. Moreover only two halo models are considered for their analysis. In an another earlier work ([24]), a neutralino dark matter in AMSB model is studied to obtain the region in scalar cross section ($\sigma_{\text{scatt}} - m_\chi$) parameter space. But in this case WMAP limit has not been taken into account. In Ref. [25], the γ signal from galactic centre region due to dark matter annihilation is addressed mainly for the case of FERMI (formerly GLAST [26]) satellite-borne experiment. Ref. [27] discusses the γ -flux from galactic centre region, originated by dark matter annihilations. The authors made the analysis with different particle dark matter candidates with reference to MSSM, Kaluza-Klein extra dimensional model etc. for different halo profiles and taking into account the Fermi-LAT experiment. But the neutrinos as dark matter annihilation products are not addressed. In another work by Allahverdi et al [28] considered MSSM and $U(1)_{B-L}$ extended MSSM model for dark matter candidate and calculated γ and neutrino fluxes from galactic and extra-galactic origins by annihilating dark matter. But they have considered only one dark matter halo profile namely NFW halo profile and they have not shown the neutrinos flux for different neutrino flavours. Moreover, no detailed comparison of their results with high energy neutrino or gamma search experiments is shown. There are also other earlier works like [29] where dark matter annihilations in galaxy are addressed.

In this work we use the mAMSB framework for the neutralino DM candidate and study both the possible γ -ray and neutrino flux that an experiment will probe in the direction of galactic centre. We perform this study for four dark matter halo profiles. The γ -ray results are compared with HESS experiment and for neutrinos,

we estimate the possible signal in ANTARES under sea detector.

The paper is organised as follows. In section 2 we discuss the calculation of relic densities of mAMSB neutralinos for the parameter space. The relic densities are then compared with the WMAP results. The parameter space thus constrained further by WMAP is then used to calculate the spin dependent and spin independent scattering cross sections. They are compared with the existing direct detection experiment limits. These are discussed in section 3. In section 4 the indirect detection of the mAMSB dark matter from their annihilations at galactic centre and halo are discussed. To this end the gamma signals and neutrino signals are addressed. Finally in section 5 we give discussions and conclusions.

2 Relic Abundance Calculation

In order to calculate the relic abundance of the LSP, χ , one needs to consider annihilation of N supersymmetric particles with masses m_i ($i=1,2,...,N$) and internal degrees of freedom g_i respectively. The relic abundance is obtained by numerically solving the Boltzmann's equation,

$$\frac{dn}{dt} + 3Hn = -\langle\sigma v\rangle(n^2 - n_{\text{eq}}^2) , \quad (2)$$

where n is the total number density of all the supersymmetric particles n_i

$$n = \sum_i n_i ,$$

and n_{eq} is the value of n when the particles for dark matter candidate were in chemical equilibrium. At this epoch the temperature T of the universe was greater than T_f ($T > T_f$), the freeze out temperature of the particle considered. At a temperature below the freeze-out temperature T_f , the particles falls out of chemical and thermal equilibrium and their co-moving number density becomes fixed or “frozen”. In Eq. 2, H denotes the Hubble parameter and $\langle\sigma v\rangle$ is the thermal average of the product of annihilation cross section and the relative velocity of the two annihilating particles.

$$\langle\sigma v\rangle = \sum_{i,j} \langle\sigma_{ij} v_{ij}\rangle \frac{n_{\text{eq}}^{(i)} n_{\text{eq}}^{(j)}}{n_{\text{eq}}^2} , \quad (3)$$

with

$$v_{ij} = \frac{\sqrt{(p_i \cdot p_j)^2 - m_i^2 m_j^2}}{E_i E_j} .$$

In the above, (p_i, p_j) and (E_i, E_j) are the momenta and energies respectively for the i th and j th particles. Defining the abundance, $Y = n/s$ [30] where s is the total

entropy density of the universe, and with the dimensionless quantity $x = m_\chi/T$, with m_χ being the mass of LSP, Eq. 2 can be written in the form

$$\frac{dY}{dx} = \frac{1}{3H} \frac{ds}{dx} \langle \sigma v \rangle (Y^2 - Y_{eq}^2). \quad (4)$$

In Eq. 4, Y_{eq} is the value of Y when $n = n_{eq}$. With Hubble parameter $H = \sqrt{\frac{8}{3}\pi G\rho}$, G being the gravitational constant, the total energy density (ρ) and the total entropy density (s) of the universe are given by [30]

$$\rho = g_{eff}(T) \frac{\pi^2}{30} T^4 \quad (5)$$

$$\text{and } s = h_{eff}(T) \frac{2\pi^2}{45} T^3. \quad (6)$$

In Eqs. 5 and 6 g_{eff} , h_{eff} are the effective degrees of freedom for the energy and entropy densities respectively. Substituting Eqs. 5, Eqs. 6 and the expression for H in Eq. 4, one obtains the evolution equation of Y as

$$\frac{dY}{dx} = - \left(\frac{45}{\pi} G \right)^{-1/2} \frac{g_*^{1/2} m_\chi}{x^2} \langle \sigma v \rangle (Y^2 - Y_{eq}^2), \quad (7)$$

where $g_*^{1/2}$ is defined as [30]

$$g_*^{1/2} = \frac{h_{eff}}{g_{eff}^{1/2}} \left(1 + \frac{1}{3} \frac{T}{h_{eff}} \frac{dh_{eff}}{dT} \right). \quad (8)$$

The expression for Y_{eq} is given by [30]

$$Y_{eq}(T) = \frac{45}{4\pi^4 h_{eff}(T)} \sum_i g_i \frac{m_i^2}{T^2} K_2 \left(\frac{m_i}{T} \right), \quad (9)$$

where we sum over all supersymmetric particles denoted by i with mass m_i and internal degrees of freedom g_i . $K_2(x)$ is the modified bessel function of the second kind of order 2. The thermally-averaged cross section, $\langle \sigma v \rangle$ must include all channels by which χ can interact, including coannihilation with other particles, in which the number densities of both species are important.

Integrating Eq. 7 from $x = x_0 = m/T_0$ to $x = x_f = m/T_f$, where T_0 is the present photon temperature (2.726° K) we obtain Y_0 (value of Y at $T = T_0$) which is needed to compute the relic density. Eq. 7 is solved numerically with the following approximations,

- 1. At small x (high T), the abundance of lightest SUSY particles (LSP) are almost in equilibrium and the temperature variation of the deviation from equilibrium abundance is negligible, i.e., $Y \approx Y_{eq}$ and $\frac{Y - Y_{eq}}{T} \approx 0$. Thus, the evolution equation reduces to,

$$\frac{d \ln(Y_{eq})}{dx} = - \left(\frac{45}{\pi} G \right)^{-1/2} \frac{g_*^{1/2} m_\chi}{x^2} \langle \sigma v \rangle Y_{eq} \delta(\delta + 2), \quad (10)$$

where δ is some small constant coming from the definition of freeze-out temperature T_f .

- 2. At temperature below T_f , equilibrium abundance, Y_{eq} falls much below Y , as seen from Eq. 7 and can be neglected in the abundance evolution equation. Thus, Y_0 is obtained from the relation,

$$\frac{1}{Y_0} = \frac{1}{Y_f} - m_\chi \left(\frac{45}{\pi} G \right)^{-1/2} \int_{x_f}^{x_0} \frac{g_*^{1/2}(x)}{x^2} \langle \sigma v \rangle dx \quad (11)$$

The relic density of LSP, in the units of critical density, $\rho_{cr} = 3H^2/8\pi G$, can be expressed as

$$\Omega_\chi = \frac{m_\chi n}{\rho_{cr}} = \frac{m_\chi s_0 Y_0}{\rho_{cr}}, \quad (12)$$

where s_0 is the present entropy density evaluated at T_0 . Finally, knowing Y_0 , we can compute the relic density of the dark matter candidate, from the relation [30],

$$\Omega_\chi h^2 = 2.755 \times 10^8 \frac{m_\chi}{\text{GeV}} Y_0. \quad (13)$$

In the above h is the Hubble constant in $100 \text{ Km sec}^{-1} \text{ Mpc}^{-1}$ unit. The WMAP survey combining with recent observations of largescale structure provides the constraints on the dark matter density $\Omega_{DM} h^2$ as

$$0.099 < \Omega_{DM} h^2 < 0.123. \quad (14)$$

where Ω_{DM} is the ratio of dark matter density to the critical density $\rho_c = 1.88 h^2 \times 10^{-29} \text{ gcm}^{-3}$.

In the present work we calculate the relic densities for the dark matter candidate neutralino in mAMSB model and compare our results with the WMAP bound. The allowed parameter space in the present SUSY model is thus extracted by WMAP results.

As mentioned earlier, the parameter space of the mAMSB model is defined by the four parameters, namely $m_{3/2}$, m_0 , $\tan \beta$ and $\text{sign}(\mu)$. The whole parameter space defined by the above parameters and constrained by the allowed region of $m_0 - m_{3/2}$ (see earlier) is used to calculate the relic density Ω_χ (or $\Omega_\chi h^2$) and the results are then compared with the WMAP results.

The relic density in the present formalism of SUSY model is computed using the code `micrOMEGAs` [31]. We thus obtain the relic density for the scanned SUSY parameter space discussed above. We find that the generated LSP neutralinos span very large range of mass. Each generated LSP neutralino mass gives rise to different annihilation cross section due to their annihilations to different standard model particles and also co-annihilation processes. We mention here that the LSP neutralino

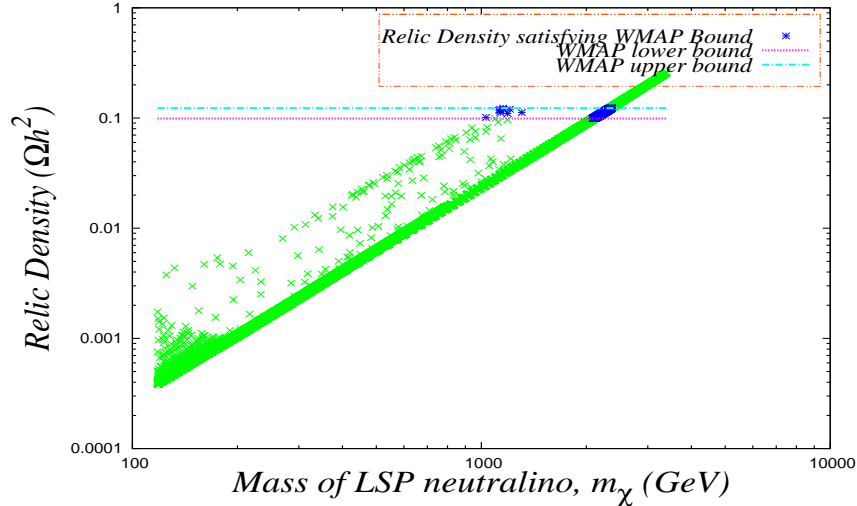


Figure 1: Scatter plot of mass of the LSP neutralino (m_χ) vs. relic density (Ωh^2) in mAMSB model. The cyan and pink line represents the WMAP upper and lower bounds on dark matter relic density respectively and the blue dotted zones corresponds to the mass range satisfying the WMAP limits.

is found to be wino dominated with the other components like bino or higgsino have very negligible contribution. The mass scales for other sparticles are above the LSP neutralino mass scale. For example for an LSP of mass ~ 2 TeV, the sneutrinos mass is ~ 14 TeV and for squark the mass scale is ~ 18 TeV; the NLSP mass is ~ 7 TeV.

In Fig. 1, the variation of relic densities for different LSP neutralino masses are shown. The scatter plots in Fig. 1 correspond to the allowed parameter space. The WMAP bound is superimposed on this scatter plot in Fig. 1 and the regions of agreement of the present calculational results with WMAP data are identified by blue coloured area in Fig. 1. From Fig. 1, we obtain two different neutralino mass regions satisfying the WMAP bound. One region is around 1 TeV and the other region is at a somewhat higher range of ~ 2 TeV.

In order to elaborate how the WMAP bound constrains the SUSY parameter space in the present mAMSB model, we make a 3-D colour coded plot in Fig. 2, where the variation of relic density Ωh^2 with the simultaneous variations of all three SUSY parameters namely $m_{3/2}$, $\tan \beta$ and m_0 are furnished. In Fig. 2, the parameters $m_{3/2}$ and $\tan \beta$ are plotted along X and Y axes respectively while the variation of gaugino mass m_0 is shown in colour coded display whereby the colour reference deep blue denotes the lower value of m_0 and increases towards the yellow zone in the plot. The corresponding variation of Ωh^2 is shown along Z axis. The WMAP limits are shown in Fig. 2 by two meshes separated by the WMAP limit along Ωh^2 axis. One observes from Fig. 2 that a very small region of the $m_{3/2} - m_0 - \tan \beta$ parameter space is allowed by WMAP. Thus WMAP limit further constraints the $m_{3/2} - m_0$

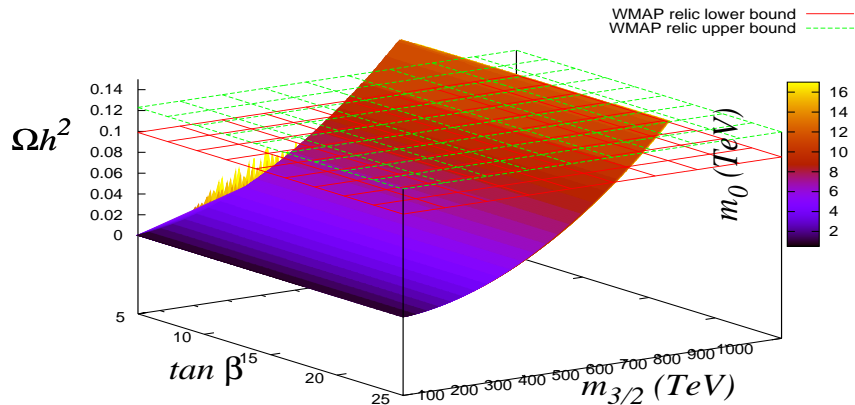


Figure 2: Constraints on SUSY parameter space from WMAP limits in present SUSY model. The gaugino mass parameter m_0 are shown by the colour index where m_0 varies from blue coloured region to yellow region as its mass increases.

parameter limits. From Fig. 2 it is also clear that only higher values of m_0 ($\sim 10 - 12$ TeV), and $m_{3/2}$ ($\sim 650 - 700$) TeV could satisfy the WMAP limits. We have not obtained any other parameter space in $m_0 - m_{3/2}$ plane that satisfy WMAP limits.

In Fig. 3, we show how the annihilation cross sections vary with the neutralino dark matter mass (m_χ) in the present model. The WMAP allowed mass region is also shown by green colour. The σv for the allowed zones (marked green) are seen to be around the value $\sim 10^{-26} \text{ cm}^3 \text{ sec}^{-1}$.

The variations of freezeout temperatures (T_f) of LSP neutralino for the mass range obtained using the SUSY parameter space discussed earlier, are shown in the scatter plot of Fig. 4. The neutralinos that satisfy WMAP relic density results are shown as blue in Fig. 4. As in Fig. 1, in this case also one observes two such regions, one is around $T_f \sim 80 - 86$ GeV (more populated) and the other (fewer candidates) is at a lower region of around $T_f \sim 40$ GeV.

3 Direct Detection

The direct detection of dark matter is based on the principle that the WIMP scatters off the target nucleus of the material of the detector causing the nucleus to recoil. The signal generated by the nuclear recoil (generally $\sim \text{keV}$) is measured for direct detection. In the direct detection experiments, attempts are made to give a bound in the $m_\chi - \sigma_{\text{scatt}}$ space (m_χ being the mass of the dark matter and σ_{scatt} is the dark matter-nucleus or dark matter-nucleon scattering cross sections). Dif-

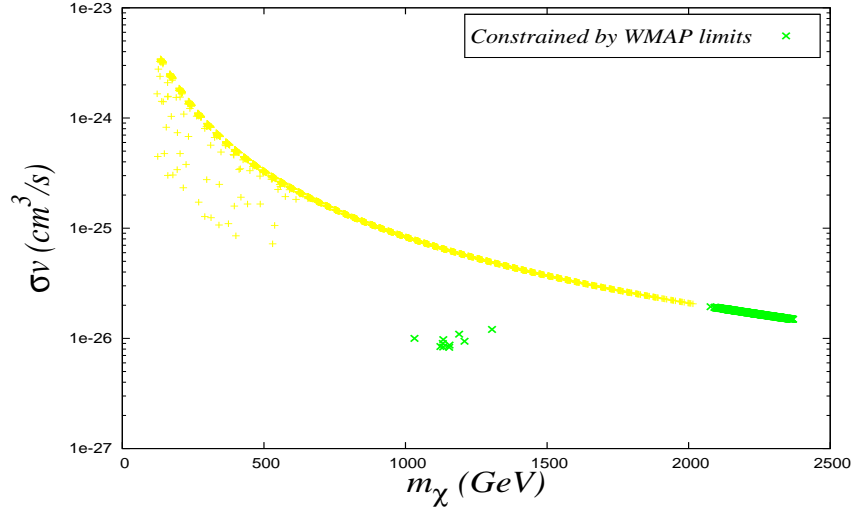


Figure 3: Plot showing the variation (in yellow) of annihilation cross section times relative velocity of annihilating neutralinos (σv) with the mass of the LSP neutralino (m_χ) in $m\text{AMSB}$ model. The green zones are the WMAP allowed regions.

ferent techniques are adopted by different direct detection experiments in order to measure the nuclear recoil energies. Some experiments that use Ge, Si or NaI as detector materials use scintillation, phonon or ionization techniques. In another class of detectors like Time Projection Chamber or TPC detectors, the drifting of ionized charges, produced by recoil nucleon of the detector material (generally noble liquids like xenon, argon and neon), produce the track from which the direction of recoil can also be measured. Some of the ongoing direct detection experiments include DAMA (NaI) [32], CDMS (^{73}Ge) [33, 34], PICASSO (CS_2) [35], XENON [36, 37], COUPP [38], LUX (use xenon) [39], CLEAN (use liquid argon and neon as scintillator) and DEAP (use argon) [40] etc. They give different limits on scattering cross sections for different dark matter mass.

The dark matter-nucleus scattering cross sections can be of two types namely axial-vector (spin-dependent) or scalar (spin-independent). The target nucleus, with zero ground state spin gives rise to spin independent interaction. On the other hand, spin-dependent interactions are for the nuclei with unpaired nucleon that gives rise to non-zero ground state spin. The experiments such as Edelweiss [41], DAMA/NaI, CDMS SuperCDMS [42], Xenon10 [36], Xenon100 [37], Zeplin [43, 44], KIMS [45], CoGeNT [46] are using detectors made of heavy nuclei (Ge or Xe) to search scalar interactions. On the other hand, NAIAD [47], SIMPLE [48], PICASSO, Tokyo/NaF [49] are using light nuclei to detect spin-dependent case.

The interaction Lagrangian for spin independent elastic scattering of Majorana

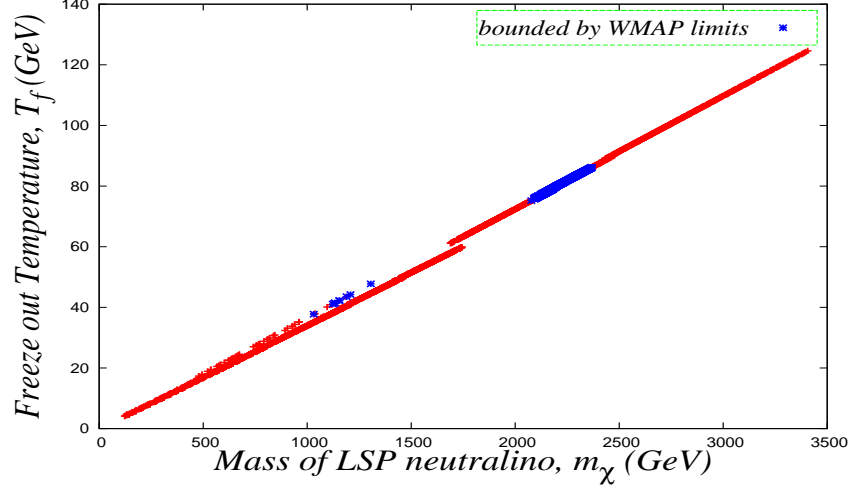


Figure 4: Plot showing the variation (in red) of freezeout temperature (T_f) with the mass of the m_{AMSB} LSP neutralino (m_χ). The blue dotted zones are constrained by WMAP limits on dark matter relic.

fermionic WIMP off nucleon N in non-relativistic limit is given by [50],

$$L_{SI} = \lambda_N \bar{\psi}_\chi \psi_\chi \bar{\psi}_N \psi_N , \quad (15)$$

where λ_N is the WIMP-nucleon coupling. Other notations have their usual significance. The interaction Lagrangian for spin-dependent case is given by [50],

$$L_{SD} = \epsilon_N \bar{\psi}_\chi \gamma_\mu \gamma_5 \psi_\chi \bar{\psi}_N \gamma^\mu \gamma_5 \psi_N , \quad (16)$$

where ϵ_N denotes the coupling. The spin-dependent and spin-independent cross sections for scattering of dark matter particle (χ) with nucleon (N) are respectively given in compact forms as,

$$\sigma^{\text{SD}} = \frac{4m_\chi^2 M_N^2}{\pi(m_\chi + M_N)^2} \times 3|A^{\text{SD}}|^2 , \quad (17)$$

$$\sigma^{\text{SI}} = \frac{4m_\chi^2 M_N^2}{\pi(m_\chi + M_N)^2} \times |A^{\text{SI}}|^2 , \quad (18)$$

where m_χ , M_N are the dark matter particle mass and nucleon mass respectively. In the above, A^{SI} and A^{SD} are the relevant matrix elements that depend on the quark contents of the target nucleon (N) for χ - N scattering.

We have computed both spin-independent and spin-dependent scattering cross sections of neutralino dark matter for a wide range of mass in this model respecting the allowed $m_0 - m_{3/2}$ bound. As the nucleon consists of both protons and neutrons, the WIMPs can be scattered off both nucleons. The contribution of loop diagrams along with the tree level diagrams have also been included for calculations of scattering amplitudes for both SI and SD cases of $\chi - N$ scattering. These scattering

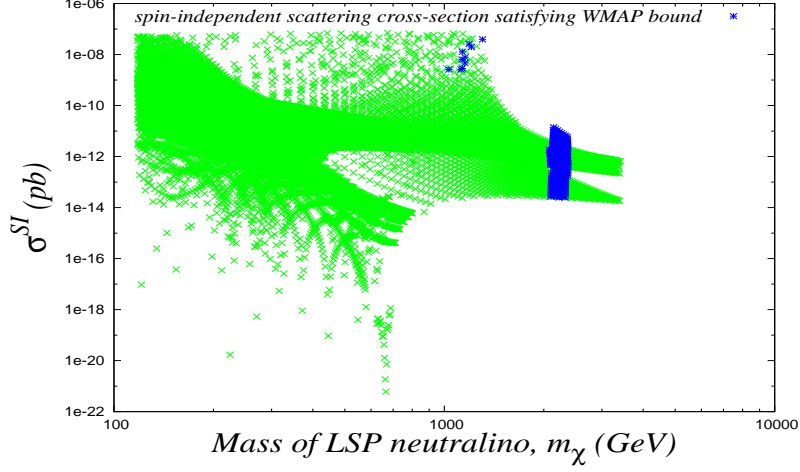


Figure 5: The plot showing the variation of Spin Independent scattering cross section (σ^{SI}) with for Mass of the LSP neutralino (m_χ) for the allowed SUSY parameter space. The blue zones are the LSP neutralinos which satisfy the WMAP relic.

cross sections for different neutralino masses are computed using `micrOMEGAs` [31] computer code. The results for both SI and SD cases are shown in Fig. 5 and Fig. 6 respectively as scattered plots for scattering with protons.

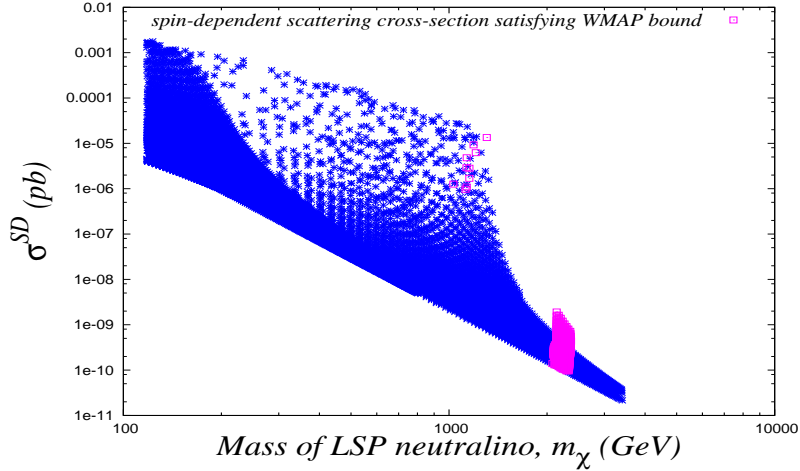


Figure 6: The variation of Spin Dependent scattering cross section (σ^{SD}) with mass of the LSP neutralino (m_χ) allowed parameter space is shown in this plot. WMAP relic satisfied two zones are shown in pink.

The green scattered plots in Fig. 5 give the spin independent scattering cross section σ^{SI} for various neutralino masses m_χ generated in the present AMSB model with the bound on parameter space. The blue scattered plots in Fig. 6, on the other hand, are for the spin dependent case. The mass region(s) in this model that satisfy the WMAP results for relic density are superimposed over these two figures in

order to constrain the $m_\chi - \sigma^{\text{SI/SD}}$ space obtained from Figs. 5, 6. The blue patches in Fig. 5 and the pink patches in Fig. 6 represent the mass regions that satisfy WMAP results. Clearly, there are two different zones allowed by the WMAP limits as expected from the discussions in Sect. 2. For the WMAP allowed lower mass region (around 1 TeV), the SI cross section (Fig. 5) extends between $\sim 10^{-9} - \sim 10^{-7}$ pb. The WMAP allowed higher mass region (around 2 TeV) which spans larger region in $m_\chi - \sigma^{\text{SI}}$ space than the WMAP allowed lower mass region, is confined within SI cross section limit $\sim 10^{-11} - \sim 10^{-14}$ pb in Fig. 5. The pink regions in Fig. 6 signify the WMAP allowed region. Here, the value of SD scattering cross section is coming to be higher than that of SI as it is expected from the theoretical perspective.

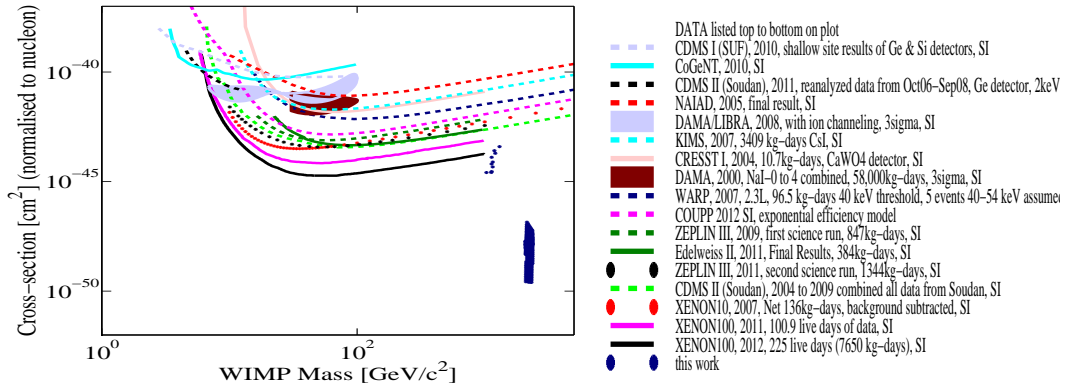


Figure 7: *Limits on spin independent scattering cross sections set by various experiments and comparison with our results in mAMSB model. Our calculated results that follow the WMAP limits are shown by two distinct blue patches in this figure and they are found to be within these experimental bounds.*

Similarly, in Fig. 6 the WMAP allowed lower mass region (around 1 TeV) constrain the spin dependent cross section σ^{SD} limits in the range $\sim 10^{-6} - \sim 10^{-5}$ pb and for the region of around 2 TeV σ^{SD} lies between $\sim 10^{-10}$ to $\sim 10^{-9}$ pb. We mentioned in passing that we obtained similar nature for WIMP-*neutron* elastic scattering.

Figs. 7 and 8 show respectively various upper limits in dark matter mass - SI or SD scattering cross section ($m_\chi - \sigma^{\text{SI or SD}}$) plane set by different ongoing direct detection experiments. The WMAP-allowed regions from the present model for neutralino dark matter are superimposed on them for comparison. The experimental limits are obtained from the compilation given in Ref. [51]. The names of the different experiments are furnished as legends in the figures. It is obvious from Figs. 7 and 8 that the allowed parameter space for the considered AMSB model is within the

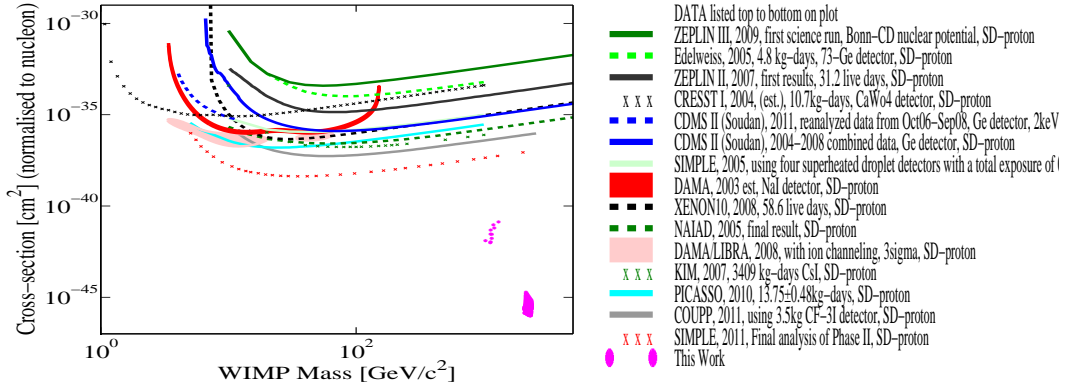


Figure 8: *Limits on spin dependent scattering cross sections set by various experiments and comparison with our calculated results. The pink zones are the satisfying WMAP bounds and they are few orders below the upper bounds of these experimental data.*

allowed limits of the experimental bounds.

4 Indirect Detection

Weakly interacting dark matter in our galaxy can be trapped inside massive heavenly bodies like galactic centre or the sun due to the gravity of these bodies. The dark matter particles, in course of their passage through such massive bodies undergo elastic scattering off the nuclei present there as a result of which their velocity deplete. If their velocities fall below their escape velocities from such massive objects, the dark matter particles are trapped. These trapped dark matter particle (χ) may undergo the process of pair-annihilation producing primarily b , c and t quarks, τ leptons, gauge bosons, etc. ($\chi\chi \rightarrow q\bar{q}, l^+l^-, \nu\bar{\nu}, ZZ, W^+W^-, \dots$). The annihilation products depend on the mass and composition of the dark matter. Neutrinos and antineutrinos can be produced by the decay of primary annihilation products or through direct annihilation.

The main principle of indirect detection of dark matter is to detect and measure the fluxes of standard model particles produced from the annihilation of dark matter trapped by the gravitation of massive heavenly bodies. Recently many new results from indirect DM searches have been released. An interpretation of these excesses related to astrophysical processes from any galactic or extragalactic sources is still not very clear. The products from the annihilation of dark matter particles in massive

bodies such as in galactic centre may explain such excess signals.

There are a lot of satellite borne experiments that look for gamma rays or anti-matters in cosmos. Some terrestrial experiments are also suited for looking at cosmic gamma rays, neutrinos etc. Such experiments include PAMELA [52] that confirms an excess in positron fraction in agreement with earlier indications by HEAT [53] and AMS01 [54]. Other satellite borne experiments like FERMI [55] and ATIC [56] report an excess in total electron and positron spectrum at energies of several hundreds of GeV's, much higher than that of PAMELA search. The cosmic gamma rays from the galactic sources and from galactic centre are measured in a wide range of energies by INTEGRAL ($< \sim 1$ MeV) [57], EGRET [58], FERMI [59], HESS [11, 12], MAGIC [60], Whipple/Veritas [61], CANGAROO ($> \sim 100$ GeV) [62] etc.

In this work we mainly focus on the gamma ray and neutrinos from dark matter annihilations in the direction at and around galactic centre (GC). The GC region has higher dark matter density and hence a promising site for the study of indirect detection of dark matter. Although GC seems to be the most obvious target, it is also one of the most difficult areas to work with because of the complex and poorly-understood backgrounds [63, 64], for signals from around GC and uncertain dark matter profile [65, 66, 67].

The galactic gravitational potential leads to a higher dark matter density at the centre of Milky Way. The expected flux from the galactic centre depends on the distribution of dark matter in the galaxy. The dark matter density profile $\rho(r)$ is assumed to be spherically symmetric. The differential flux of the outgoing particle of type i is given by

$$I^i(E, \theta) = \frac{d\Phi_i}{dE} = \sum_j \frac{\sigma_j v}{8\pi\alpha m_\chi^2} \frac{dN_j^i}{dE}(E) J(\theta, \Delta\Omega) \quad (19)$$

where the factor, α is 1 or 2 depending on whether the assumed WIMPs are self-conjugated or not respectively. In the above 'j' denotes a particular annihilation channel. It is also to be mentioned that the effect of this factor, α on the above differential flux is much less significant in comparison to the dark matter density fluctuations in the innermost regions of Milky Way. Here we consider α to be unity as the neutralinos from the mAMSB model (the dark matter candidate chosen in the present work) are self-conjugated. In Eq. 19, σ is the annihilation cross section of dark matter and v denotes the relative velocity of the dark matter particles. The quantity $\frac{dN_j^i}{dE}(E)$ in Eq. 19 is the energy spectrum of particle i and $J(\theta, \Delta\Omega)$ is given by,

$$J(\theta, \Delta\Omega) = \int_{\Delta\Omega} d\Omega \int_{\text{line of sight}} \langle \rho^2(r(\tilde{r}, \theta)) \rangle d\tilde{r} . \quad (20)$$

With θ being the angle subtended by the line of sight of an observer on the earth (along the length \tilde{r}) on R_\odot – the distance between GC and the terrestrial observer

(in solar system). The source to observer distance \tilde{r} can be calculated as

$$\tilde{r} = \sqrt{(r^2 + R_\odot^2 - 2rR_\odot \cos\theta)} , \quad (21)$$

In the above, the target region is considered to be at a distance r from GC (at the GC, $r = 0$). Here we also mention that the GC is assumed to be coincident with the halo centre). The solar system's position in the halo from the GC is given by $R_\odot = 8.0$ kpc. In Eq. 20, $\Delta\Omega$ is the solid angle over which the observation is to be made and $\rho(r)$ is the dark matter density at a distance r from GC. Clearly the integration on the RHS of Eq. 20 is along the line of sight. Thus the astrophysical factor J in Eq. 19 has only a θ dependence (along with $\Delta\Omega$) and thus the differential flux I_γ can be expressed in terms of the angle θ corresponding to different positions of the source in galactic halo with respect to GC.

The dark matter density $\rho(r)$ is related to the spherically symmetric halo profile of galactic dark matter by the equation

$$\rho(r) = \rho_0 F_{\text{halo}}(r) , \quad (22)$$

where ρ_0 is the dark matter density at the galactic centre assumed to be 0.3 GeV/cm^3 and $F_{\text{halo}}(r)$ is the halo profile of the galactic dark matter which can be expressed in a parametric form,

$$F_{\text{halo}}(r) = \left[\frac{R_\odot}{r} \right]^\gamma \left[\frac{1 + \left[\frac{R_\odot}{a} \right]^\alpha}{1 + \left[\frac{r}{a} \right]^\alpha} \right]^\alpha \frac{\beta-\gamma}{\alpha} . \quad (23)$$

In the above, a is a scale parameter and the other parameters α, β, γ take different values for different halo models which follow the above parametric form for F_{halo} . For example, for NFW halo profile [68], $\alpha = 1, \beta = 3, \gamma = 1$ and $a = 20$ kpc, whereas the parameter set $\alpha = 2, \beta = 2, \gamma = 0$ and $a = 4$ kpc represents isothermal profile with core [69]. Again for the Moore profile [70] we have, $\alpha = 1.5, \beta = 3, \gamma = 1.5$ and $a = 28$ kpc. In Einasto halo profile [71] however, a different kind of parametric form is adopted which is given by,

$$F_{\text{halo}}^{\text{Ein}}(r) = \exp \left[\frac{-2}{\tilde{\alpha}} \left(\left(\frac{r}{R_\odot} \right)^{\tilde{\alpha}} - 1 \right) \right] , \quad (24)$$

where $\tilde{\alpha}$ is the parameter. In this work $\tilde{\alpha} = 0.17$ is adopted. In what follows the four profiles are referred to as NFW, Isothermal, Moore and Einasto respectively. The galactic halo densities for these four halo models are shown in Fig. 9. In the present work we show the gamma ray and neutrino flux from galactic centre region for each of the four halo profiles mentioned above.

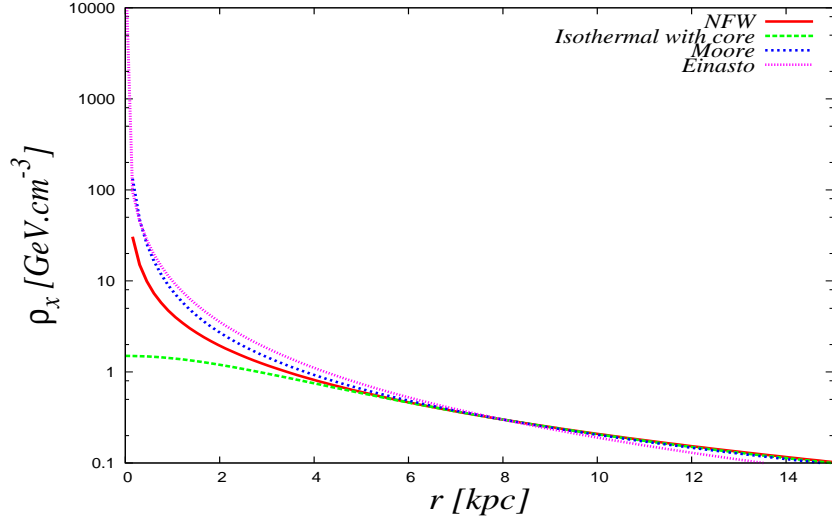


Figure 9: *The variation of galactic halo density with radial distance for various halo models and the cuspy or flat nature of the considered halo profiles are shown.*

4.1 Gamma Ray Flux Results

There are generally two kinds of γ -ray emission from DM annihilation. In the first category γ is produced directly from the annihilation final state particles which is called primary emission in which final charged leptons emit gamma ray or π^0 which eventually decays to gamma ray after hadronization. The other kind is called secondary emission in which gamma rays are produced by interactions of final state particles with external medium or radiation field such as the inverse Compton effects etc. Here we consider only the first type of emission for which the relation (19) holds. Here we calculate the gamma ray flux from the galactic centre as also from other places in galactic dark matter halo along the line of sight around the GC. As discussed in the previous section, the targets away from the galactic centre are characterised by changing only the angle θ . This angle θ in fact denotes the angle of sight from the observer with respect to the line of sight when the observer is looking directly at the galactic centre. The polarisation effect of final state gauge bosons (W^\pm and Z) and also the photon radiation effect which strongly affect the gamma ray spectra are also taken into account in the present work. The γ -flux is computed using `micrOMEGAs` code. The calculations are made for each the four halo profiles, referred to as NFW, Isothermal, Moore and Einasto and the results are furnished in the four figures namely Figs. 10a - 10d respectively.

In Figs. 10a - 10d, we plot the quantity $E^2 \times \frac{d\Phi}{dE}$ for different values E , the energy of the emitted γ rays from dark matter annihilations. We show the results for the cases when $\theta = 0$ (galactic centre), $\theta = 30^\circ$ and $\theta = 60^\circ$ and are shown as red, green and blue regions respectively. One notices in Figs. 10a - 10d that γ flux

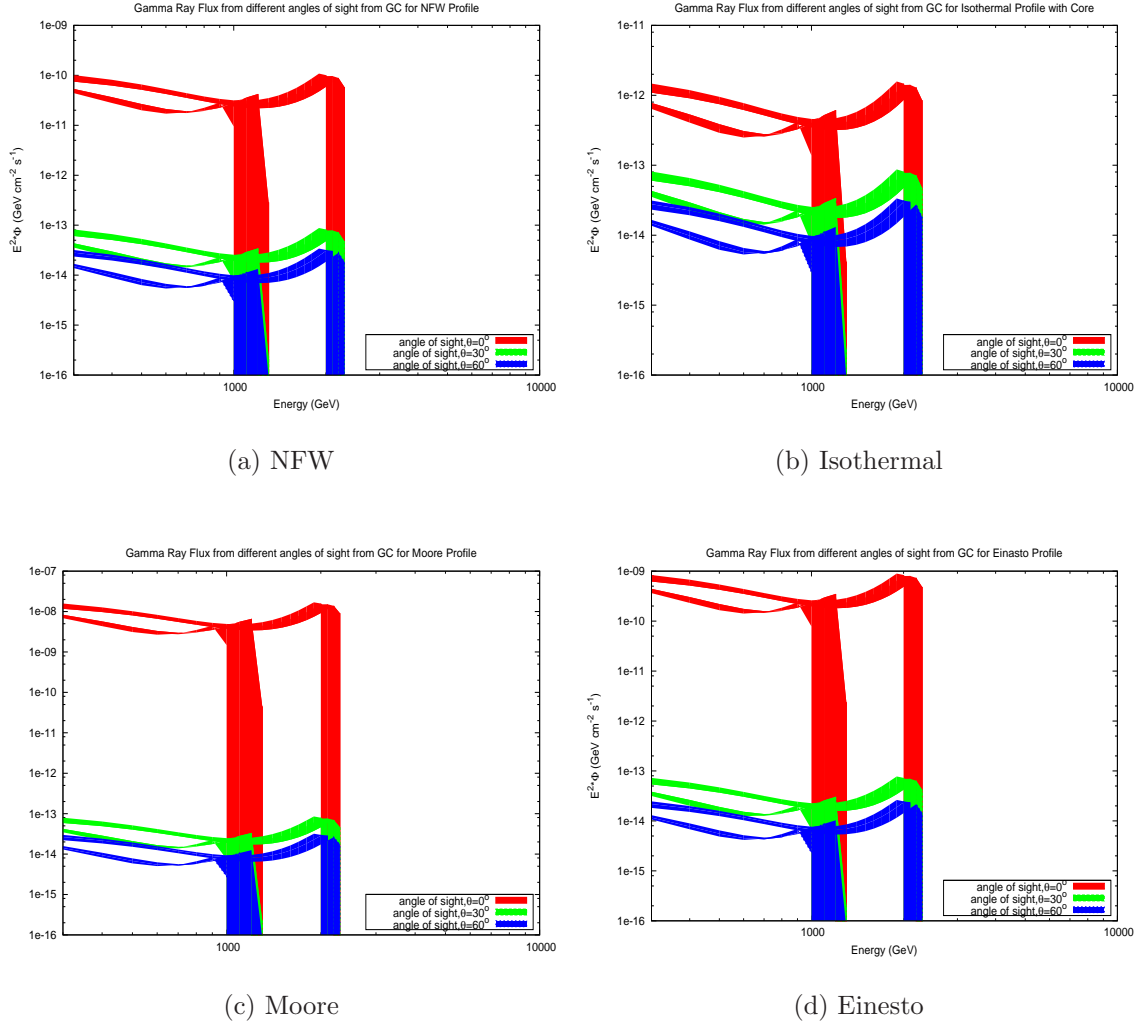


Figure 10: Plot showing the variation of gamma ray flux with energies from the annihilation of dark matter for different galactic DM halo models and for different angles of sight, θ . The red lines describe the flux observed at $\theta = 0^\circ$, i.e., from the galactic centre and the green and blue coloured regions are for the observations at $\theta = 30^\circ$ and 60° respectively. The subfigures are for different commonly used dark matter halo profiles implemented in this work, a) NFW profile b) Isothermal profile with core c) Moore profile d) Einasto profile

for any particular value of the angle θ are given as a pair of plots designated by the specific colour code (red, blue or green), assumed for the results corresponding to that particular θ . This is due to the fact that the WMAP data constrain the supersymmetric parameter space considered in this work, in two distinct zones as shown in Figs. 1, 2 and each of the plots in every such pair of γ flux in Figs. 10a - 10d correspond to each of the WMAP allowed regions for the present AMSB model

for cold dark matter candidates. It is clear from Figs. 10a - 10d that calculations with different halo profiles yield different results for γ flux. It is also to be noted that the flux in the direction of the galactic centre ($\theta = 0$) is larger than the flux from other directions (corresponding to different values of $\theta \neq 0$) for each of the four halo models considered.

The γ fluxes are found to be almost of the similar order for the cases when $\theta = 30^\circ$ and $\theta = 60^\circ$ in each of the Figs. 10a - 10d. This reflects the fact that the DM halo profiles are almost flat in those regions. The Einasto profile has a finite (zero) central slope unlike the NFW profile which has a divergent (infinite) central density. As it is not yet known which model provides the best description of the central densities of simulated dark-matter halos, we have taken these known models into account.

The γ -flux thus obtained for different halo models are compared with the observational results of The High Energy Stereoscopic System (HESS) experiment. Located in Namibia, the HESS experiment is designed to investigate high energy cosmic gamma rays (~ 100 GeV - TeV energy ranges) and it can also investigate the γ -rays in its observable energy range which can be due to the annihilation of cold dark matter particles. The results are given in Fig. 11 and Fig. 12. In each of the figures, the calculated flux are shown by two different regions corresponding to WMAP constrained two zones of dark matter mass in the present mAMSB model (discussed earlier). It has been argued by Prada *et al.* in Ref. [72] (and also in Ref. [73]) that due to the infall of baryons at the galactic centre, the expected γ signal from dark matter annihilation at galactic centre will be boosted in case the dark matter consists of supersymmetric particles. In fact, considering neutralino in minimal supergravity (mSUGRA) model as the candidate for dark matter and with the NFW dark matter halo profile, they have demonstrated that the said boost can be of the order of 1000. In Fig. 11a, the γ flux from the galactic centre as calculated from the annihilation of neutralino dark matter in present mAMSB model assuming the NFW profile, is compared with the HESS results. The solid angle at which the HESS experiment looks at the galactic centre is $\sim 10^{-5}$ sr, a value which is also adopted in the present calculations to obtain the results shown in Fig. 11 and Fig. 12. It is evident from Fig. 11a that the γ -flux obtained from the present calculations is much less than the HESS results for the energy range given by the model with WMAP constraints. In Fig. 11b we show a representative plot where the calculated γ -flux is multiplied (“boosted”) by a factor of 1000 and then compared with the HESS results. Fig. 11b shows that the “boosted” flux is in the similar ball park of HESS results which seems to satisfy the claim made in Ref. [72]. In Figs. 12a, 12b and 12c, we show similar comparisons with HESS results for calculations made with Einasto, Moore and isothermal halo profiles respectively. One observes from Fig. 12 that both for isothermal and Einasto profiles, the calculated fluxes are below the HESS results

while for Moore profile, they are comparable with HESS results. Both NFW and Moore profiles are cuspy in nature and they essentially differ by the values of the parameters α , β , γ . On the other hand both the Einasto and isothermal profiles are non-cuspy in nature while the latter is a flat halo profile. One needs to increase the calculated flux by a factor $\sim 10^2$ for the former case while the calculated flux for the isothermal profile needs a boost of $\sim 10^5$ to be in the regime of HESS observational results.

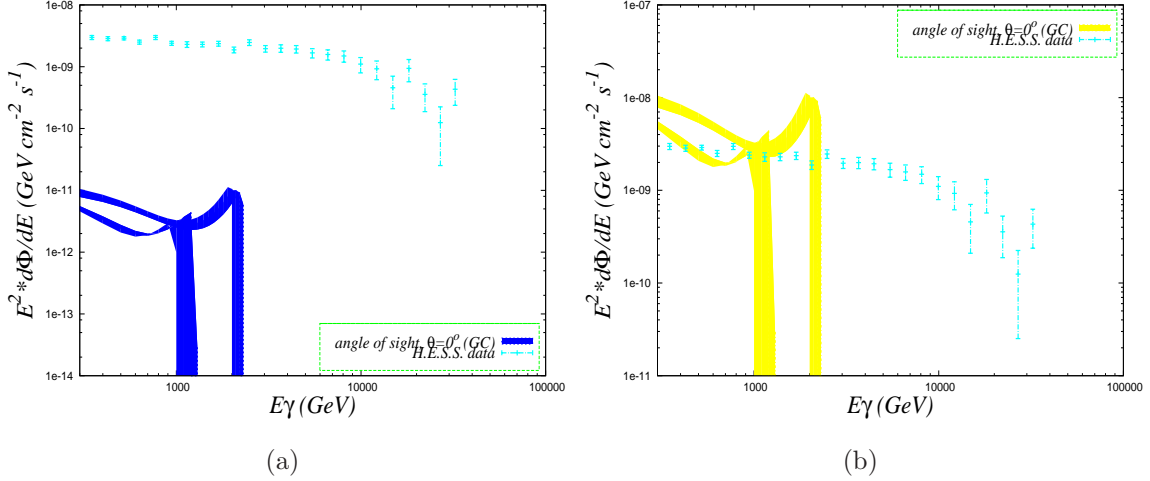


Figure 11: Plot of energy vs. γ flux for dark matter annihilation at the galactic centre and comparison with the HESS experimental data for NFW profile a) without baryonic compression and b) with the baryonic compression and $\sim 10^3$ flux enhancement

4.2 Neutrino Flux Results

As discussed earlier, neutrinos can also be produced by the annihilation of two neutralinos – the present dark matter candidate. These trapped dark matter at the galactic centre produces primarily b , c , t quarks, τ leptons, gauge bosons, etc. through the process of pair-annihilations. The neutrinos can be obtained from the decay or pair annihilation of the primary products. The neutrinos can also be produced directly from the annihilation of two mAMSB neutralinos ($\chi\tilde{\chi} \rightarrow \nu\bar{\nu}$) mediated by Z , sneutrino ($\tilde{\nu}$) etc. In this work we investigate the muon neutrino (ν_μ) flux from the galactic centre due to the annihilation of such neutralinos in the present mAMSB model and its possible detection prospect at an earthbound detector. Searches for neutralino annihilation into neutrinos is subject to extensive experimental investigations in view of the neutrino telescopes like IceCube [74], Baikal [75], NESTOR [76], ANTARES [18]. The calculation of flux of neutrinos coming from GC are similar to

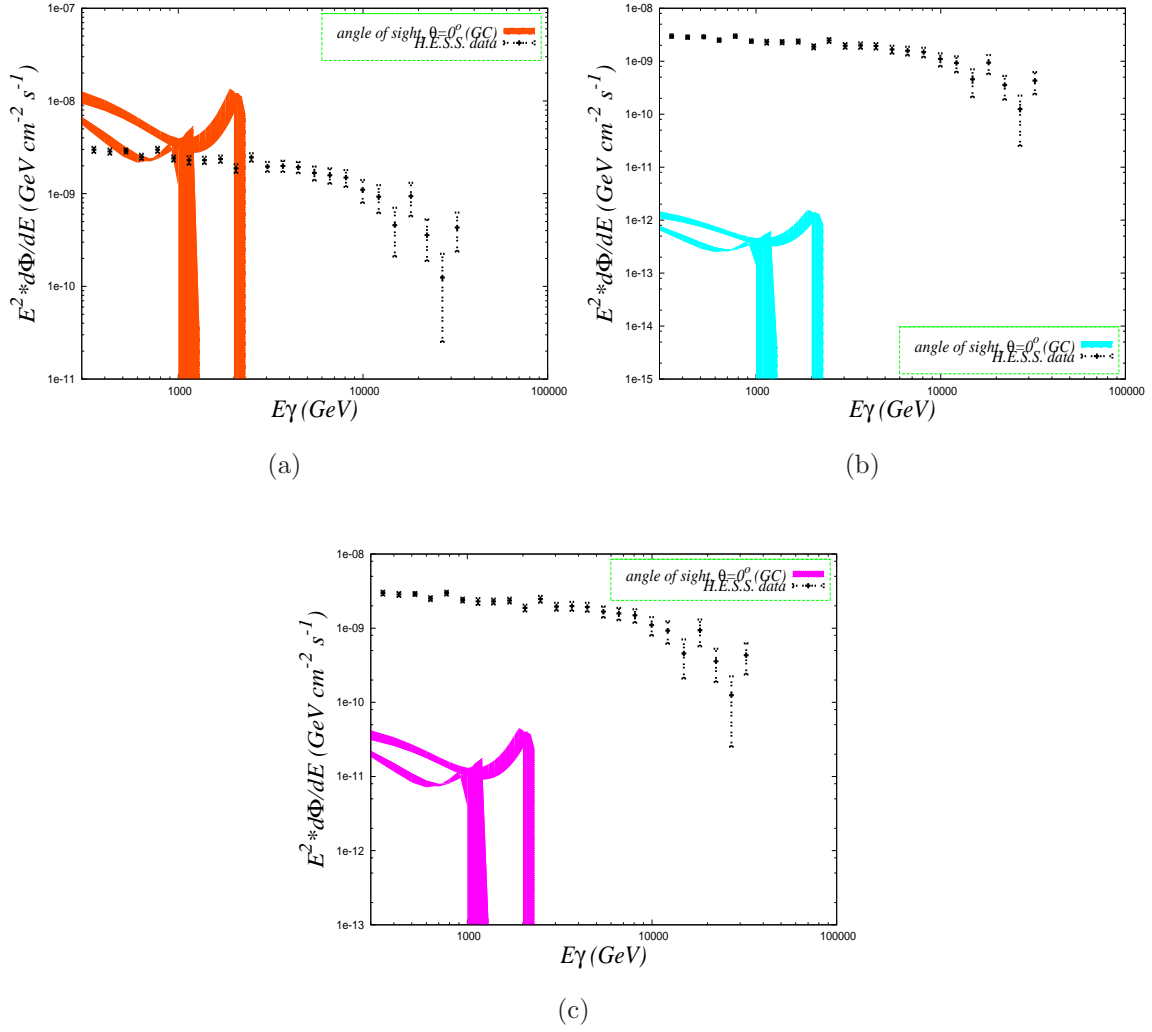


Figure 12: Plot of energy vs. γ flux from DM annihilation at the GC and comparison with the HESS experimental data for a) Moore profile, b) Isothermal profile with core and c) Einasto profile

that of gamma rays as both are electromagnetically neutral particles. So, they are not affected by the irregularities of galactic magnetic fields or any magnetic turbulences. Also, they do not suffer any energy loss from inverse compton effect or from synchrotron radiation. For the present case we calculate the possible muon (μ) signal from these neutrinos at ANTARES neutrino telescope [18] installed in the sea-bed off France coast.

We use `micrOMEGAs` computer code to calculate the neutrino flux in the direction of the galactic centre for all the four halo models considered. The neutrino flux for the halo models can be obtained using similar equations (Eqs. 19 - 23) that is used for obtaining γ -flux. The ν -flux for each of the three flavours namely ν_e , ν_μ and ν_τ are

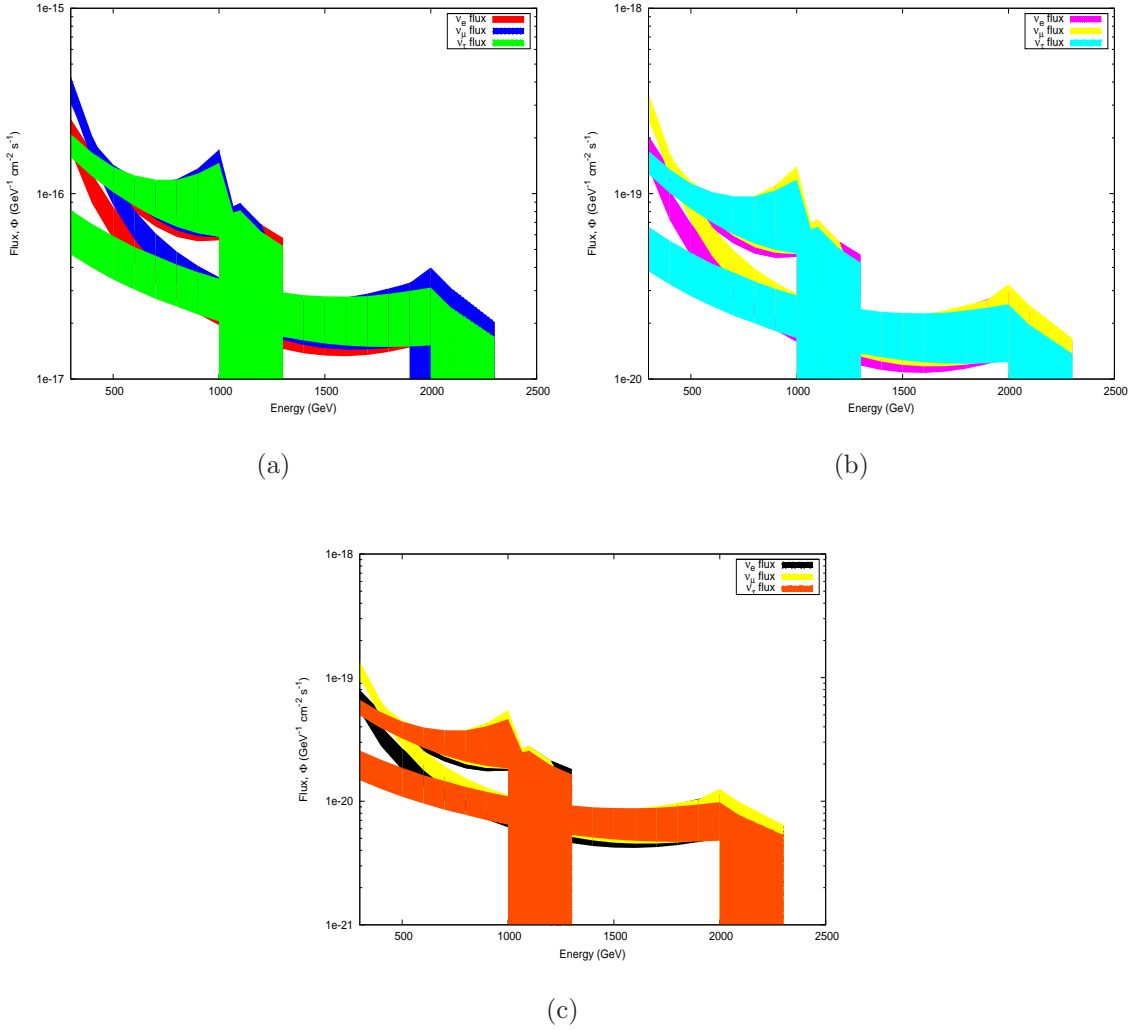


Figure 13: *Neutrino flux of three flavours (ν_e , ν_μ and ν_τ) for different energies for a) angle of sight, $\theta = 0^\circ$ b) angle of sight, $\theta = 30^\circ$ and c) angle of sight, $\theta = 60^\circ$ from the galactic centre respectively.*

calculated separately for three values of the angle θ (Eq. 19 and discussions earlier) namely $\theta = 0^\circ$, $\theta = 30^\circ$, $\theta = 60^\circ$. The results are furnished in Figs. 13 - 16. In Fig. 13, we give results only for NFW profile for the two allowed regions of dark matter mass around 1 TeV and around 2 TeV. We have done similar calculations for other three profiles namely Einasto, Isothermal and Moore halo profiles. As seen from Fig. 13, the big overlap regions of the plots for the two allowed mass zones reduce their clarity and readability. Therefore in Figs. 14 - 16, we plot the neutrino fluxes for energies upto 1000 GeV for the two allowed dark matter mass regions discussed earlier.

The three figures namely Fig. 14, Fig. 15 and Fig. 16 correspond to $\theta = 0^\circ$, 30°

and 60° respectively. In these figures the ν_e flux, the ν_μ flux and the ν_τ flux are shown respectively by red, blue and green colours in Fig. 14, pink, yellow and turquoise colour labels in Fig. 15 and black, yellow and orange colours in Fig. 16 respectively. The two flux regions for each of the neutrino flavours are for the two different allowed dark matter mass zones in this model obtained from WMAP results. The ν flux for different dark matter profiles considered here, exhibit similar trends as for the case of γ flux in the sense that the flux is more for Moore profile and gradually decreases for Einasto, NFW and isothermal profiles.

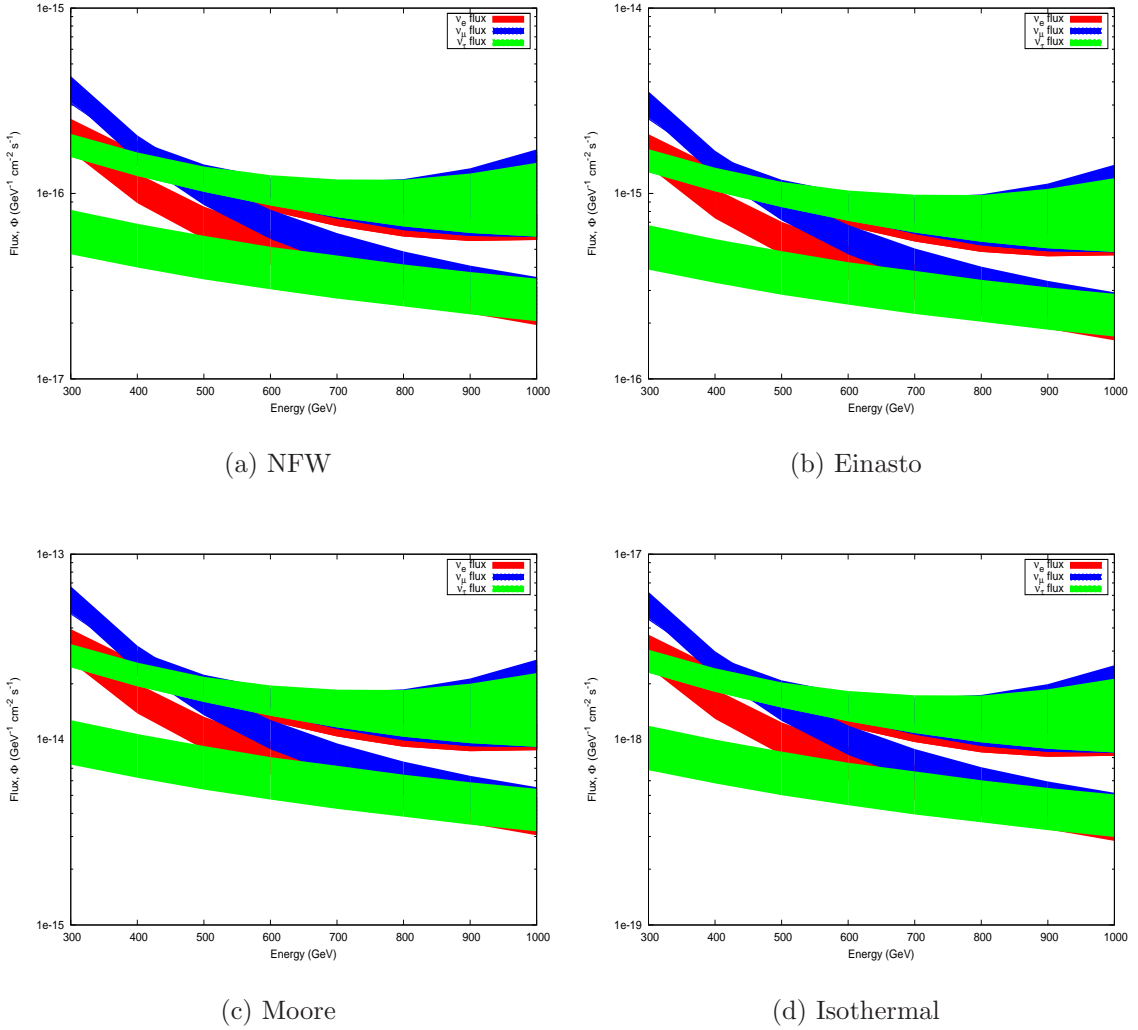


Figure 14: *neutrino flux for three flavours (ν_e , ν_μ and ν_τ) for different energies from the annihilation of dark matter at from the galactic centre. The red, blue and green patches describe the fluxes corresponding to ν_e , ν_μ and ν_τ respectively*

The neutrinos, while reaching the earth from the galactic centre will undergo flavour oscillations, whereby the flux of a particular flavour, say ν_μ , will be modified

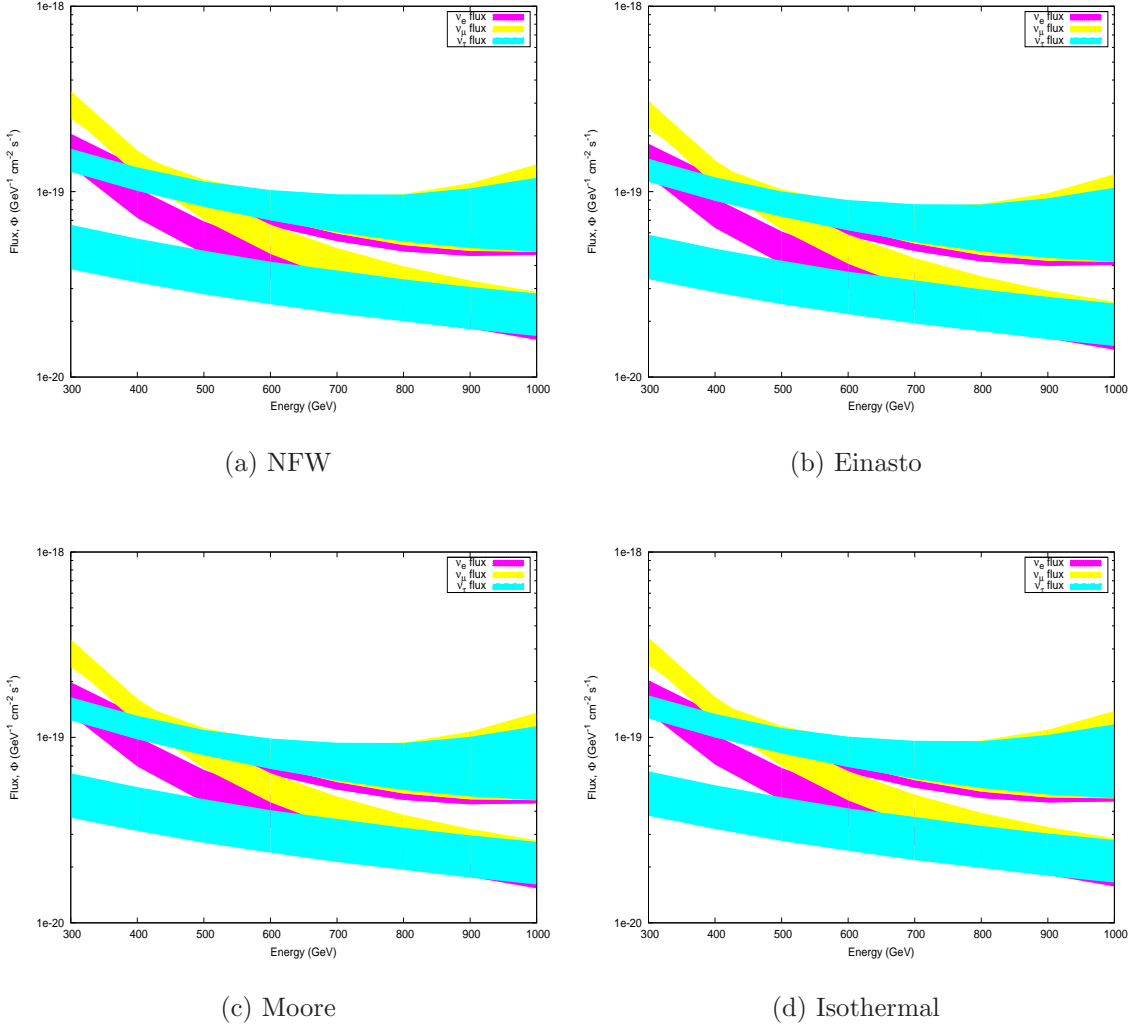
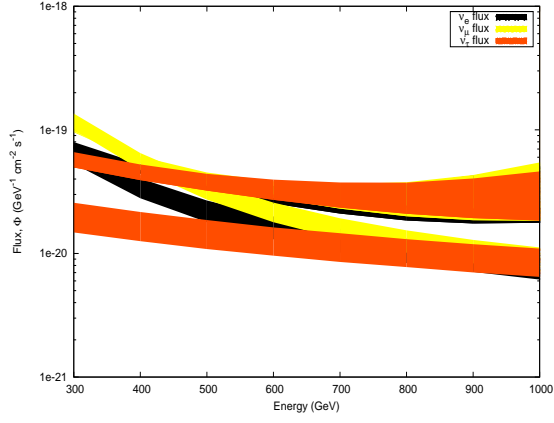


Figure 15: *neutrino flux of three flavours (ν_e , ν_μ and ν_τ) for various energies for angle of sight, $\theta = 30^\circ$ from the galactic centre. The pink, yellow and cyan coloured zones describe the fluxes corresponding to ν_e , ν_μ and ν_τ respectively*

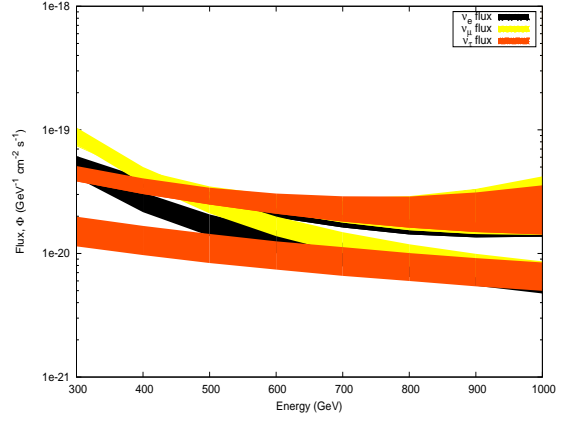
on reaching the earth from the galactic centre. Since the baseline length L is very large in this case in comparison to oscillation length, the oscillation part is averaged out. Thus in the limit $L \rightarrow \infty$, the probability that a neutrino with flavour α will oscillate to flavour β is given by

$$\begin{aligned}
 P(\nu_\alpha \rightarrow \nu_\beta; L = \infty) &= \delta_{\alpha\beta} - \sum_{i \neq j} U_{\alpha i}^* U_{\beta i} U_{\alpha j} U_{\beta j}^* \\
 &= |U_{\alpha i}|^2 |U_{\beta i}|^2,
 \end{aligned} \tag{25}$$

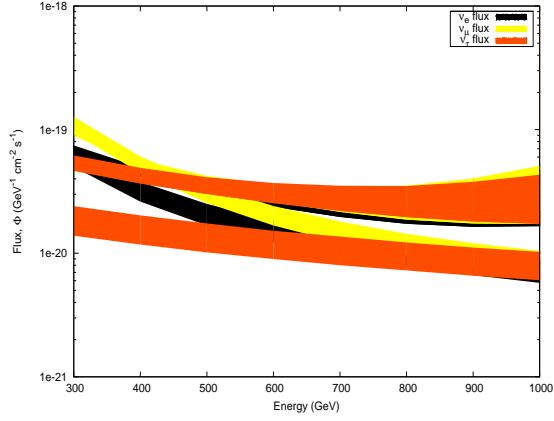
where α, β denote different flavour indices, e, μ or τ and $i, j = 1, 2, 3$ denote the mass indices of three neutrinos. In the above, the oscillation part ($\sim \Delta m_{ij}^2 (L/E)$) is averaged out due to large L/E ($\sim 10^{13}$ km/GeV). The mass-flavour mixing matrix



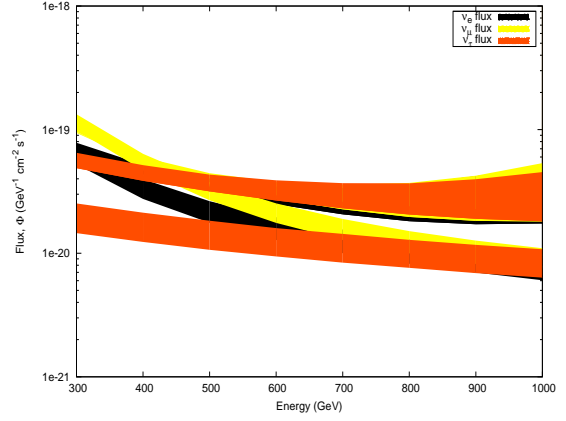
(a) NFW



(b) Einasto



(c) Moore



(d) Isothermal

Figure 16: *neutrino flux of three flavours (ν_e , ν_μ and ν_τ) for different energies for angle of sight, $\theta = 60^\circ$ from the galactic centre. The black, yellow and orange regions describe the fluxes corresponding to ν_e , ν_μ and ν_τ respectively*

U is denoted by

$$|\nu_\alpha\rangle = \sum_i U_{\alpha i} |\nu_i\rangle \quad (26)$$

and

$$U \equiv \begin{pmatrix} U_{e1} & U_{e2} & U_{e3} \\ U_{\mu1} & U_{\mu2} & U_{\mu3} \\ U_{\tau1} & U_{\tau2} & U_{\tau3} \end{pmatrix} \quad (27)$$

In fact U is the usual MNS mixing matrix given by

$$U = \begin{pmatrix} c_{12}c_{13} & s_{12}s_{13} & s_{13} \\ -s_{12}c_{23} - c_{12}s_{23}s_{13} & c_{12}c_{23} - s_{12}s_{23}s_{13} & s_{23}c_{13} \\ s_{12}s_{23} - c_{12}c_{23}s_{13} & -c_{12}s_{23} - s_{12}c_{23}s_{13} & c_{23}c_{13} \end{pmatrix}. \quad (28)$$

In the above, s, c denote $\sin \theta, \cos \theta$ respectively and θ_{12}, θ_{23} and θ_{13} are three mixing angles for three neutrino species. We consider here no CP violation in neutrino sector. From Eq. 25 probability P can be written as

$$P \equiv XX^T \quad (29)$$

where the matrix X is given by

$$X \equiv \begin{pmatrix} |U_{e1}|^2 & |U_{e2}|^2 & |U_{e3}|^2 \\ |U_{\mu1}|^2 & |U_{\mu2}|^2 & |U_{\mu3}|^2 \\ |U_{\tau1}|^2 & |U_{\tau2}|^2 & |U_{\tau3}|^2 \end{pmatrix}. \quad (30)$$

Hence, the oscillated flux of the neutrinos (of three flavours) at the detector is given by

$$\begin{pmatrix} \phi_{\nu_e} \\ \phi_{\nu_\mu} \\ \phi_{\nu_\tau} \end{pmatrix} = XX^T \begin{pmatrix} \phi_{\nu_e}^0 \\ \phi_{\nu_\mu}^0 \\ \phi_{\nu_\tau}^0 \end{pmatrix}, \quad (31)$$

where the quantities in the RHS with superfix 0 denote the initial neutrino fluxes.

In the present work we estimate the muon yield for such a ν_μ flux from galactic centre at ANTARES neutrino detector. ANTARES is a deep sea neutrino telescope and is basically a water Cerenkov detector, which detect the neutrinos by detecting the Cerenkov light of a charged lepton that is produced by the charged current scattering of neutrino off the sea water. The telescope consists of several vertical strings of around 350 metres long, each of which is fixed with 75 optical modules containing photomultiplier tubes. The strings are installed at the Mediterranean sea bed at a depth of around 2.5 Km off the French coast of Toulon. Designed to detect neutrinos with high energy (~ 100 GeV to ~ 100 TeV) of generally cosmic origin, this telescope looks in the direction of southern hemisphere. In fact due its position, ANTARES is very much suitable for observing the galactic plane and the galactic centre. In the present context, the dark matter mass from AMSB model that is allowed by WMAP, is in the region of ~ 1 TeV - ~ 2 TeV and since neutrinos from the annihilation of such dark matter at galactic centre is being studied, this telescope is best suited for the purpose.

The spectrum of muon yield, $\Phi_\mu(E_{\nu_\mu})$, for different enrgies E_{ν_μ} at ANTARES can be estimated using the relation

$$\Phi_\mu(E_{\nu_\mu}) = \phi_{\nu_\mu} A_{\text{eff},\nu}(E_{\nu_\mu}), \quad (32)$$

where, $A_{\text{eff},\nu}$ is the neutrino effective area for ANTARES telescope and is obtained from Ref. [18].

The ν_μ flux, ϕ_{ν_μ} , at the earth from the galactic centre is calculated using Eqs. 25 - 31 with $\phi_{\nu_\mu}^0$, the flux at the source, given in Fig. 14 for different halo profiles. Note that, $\phi_{\nu_\mu}^0$ at galactic centre is considered only for the case $\theta = 0$ (see earlier in this section) in the present calculation. The values of three neutrino mixing angles in Eq. 28 are taken to be $\theta_{12} = 34.0^\circ$ [77], $\theta_{23} = 46.1^\circ$ [77] and $\theta_{13} = 9.2^\circ$ [78]. The results for estimated yield of muon spectrum $\Phi_\mu(E_{\nu_\mu})$ at ANTARES is shown in Fig. 17 for all the four halo profiles considered. The estimates are shown for 5 year run of the telescope. It is seen from Fig. 17, that while NFW profile predicts very large yield, the same using the isothermal profile is rather low. The NFW profile has a cuspy structure whereas the isothermal profile gives a flat halo.

If ANTARES detects ν_μ from galactic centre then the μ signal from such detection can be compared with the results given in Fig. 17 for different DM halo profiles. Such comparison could readily give an idea of the dark matter halo profile as also the viability of the present model for DM candidate. Thus these observations can be used to probe the nature of the halo profile and the particle physics model of the dark matter as well.

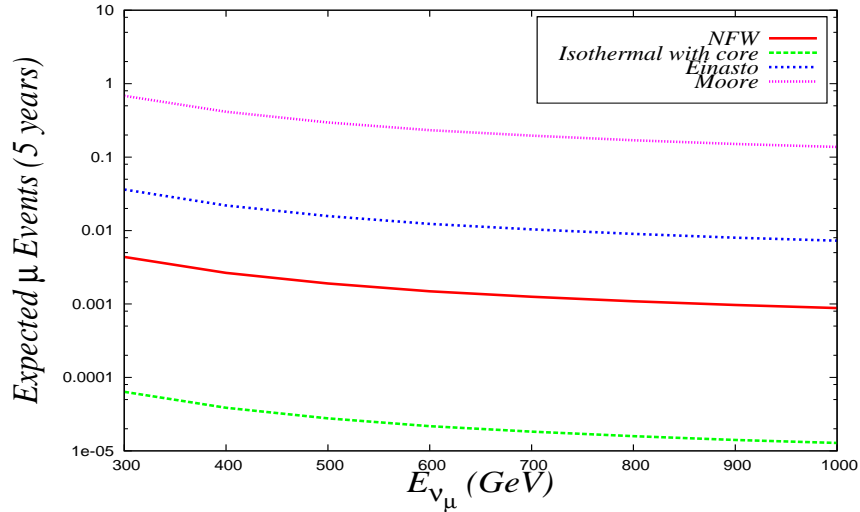


Figure 17: Estimated μ events for five year run at ANTARES neutrino telescope for different ν_μ energies obtained from dark matter annihilations at the galactic centre in the framework of mAMSB model.

5 Summary and Conclusion

In this work, we have investigated the phenomenological implications of dark matter coming from a very well known SUSY breaking model, namely minimal anomaly mediated supersymmetry breaking (mAMSB) model. The suitable candidate in this model is the neutralino stabilised by the conservation of R-parity in SUSY theory. We have randomly scanned the parameter space of this model within the theoretical bounds of the parameter space of this model and for each point in parameter space, we obtain a neutral stable candidate (neutralino) of dark matter. In doing so, latest bound on the chargino mass as given by the ATLAS collaboration is adopted.

The mass of the LSP neutralino in the present scenario is obtained in two regions of which one is around 1 TeV and the other is at a somewhat higher range of ~ 2 TeV. We have checked that these neutralinos are predominantly of wino type. The measure of the naturalness which is expressed in terms of the commonly used fine tuning parameters are obtained for the constrained neutralino masses (vide earlier) in the present scenario,

$$\begin{aligned} \frac{\delta M_Z^2}{M_Z^2}(\mu^2) &\sim 10^4, & \frac{\delta M_Z^2}{M_Z^2}(B_\mu) &\sim 10^3 \\ \frac{\delta M_t}{M_t}(\mu^2) &\sim 10^4, & \frac{\delta M_t}{M_t}(\mu^2) &\sim 10^3, \end{aligned}$$

where the symbols have their usual significance.

We calculate the relic densities of such neutralinos and compare them with WMAP bounds to obtain the mass zones of these mAMSB neutralinos that satisfy WMAP limits. The allowed parameters determined from such constraints are then used to study the direct and indirect detections of the proposed dark matter candidate, neutralino, in the present mAMSB model.

The scattering cross sections for the dark matter particles scattered off the nucleus of the detecting material are determined by the nuclear form factors and the dark matter-nucleon coupling. The two types of cross sections, namely spin independent (zero nuclear spin at the ground state) and spin dependent, are determined by the different form factors and dark matter-nucleon couplings. We calculate both the spin dependent and spin independent scattering cross sections with the constrained zone(s) of the present neutralino dark matter parameter space and hence compared our results with several recent ongoing direct detection experimental results. The calculated mass-cross sections, thus calculated, are found to be below the upper limits of many well known experiments. From experimental point of view, the future advanced direct detection techniques may probe those regions in mass-cross section plane given from the model.

We have computed the gamma ray flux coming from the galactic centre and its neighbourhood, considering that they are produced from the annihilation of dark

matter in mAMSB model. For this reason, we have taken several well known theoretically motivated dark matter halo profiles such as NFW profile, Moore profile, isothermal profiles with core and Einasto profiles and calculate the flux coming from different positions of the halo plane. As the allowed mass of the neutralino (dark matter) is high (\sim few GeV to $\sim 10^3$ GeV), the energies of the gamma rays from dark matter annihilations are also of that order. Therefore high energy gamma ray search experiments may verify the present model. For this purpose, we have chosen the HESS experiment and compared our results for different halo profiles considered, with the observed γ -flux of this experiment. In the passing we also mention that another water \hat{C} erenkov detector namely HAWC (High-Altitude Water Cherenkov Gamma-Ray Observatory) [79] near Puebla, Mexico can also detect gamma ray annihilation signal in the energy domain of $1 \sim 2$ TeV. But as mentioned, in this work we consider only HESS experiment. We find that the γ -fluxes for non-cuspy profiles like isothermal profile (flat) and Einasto profile, are orders below the HESS results whereas the cuspy profiles like Moore profile overestimate the HESS result. Calculations using the other cuspy profile, namely the NFW profile requires a boost of $\sim 10^3$ for comparison with HESS results. The Moore profile has an asymptotic slope, $\alpha = 1.5$, while the same for the NFW profile is $\alpha = 1.0$. Thus the former is steeper than the latter. Cuspy nature appears to influence the result. It is still a matter of investigation to understand whether halo profile at the galactic centre has a flat profile or a steep profile. The present analysis, within the framework of mAMSB model for dark matter candidate, seems to suggest that the cuspy nature of the profile appears to explain the HESS data better than the flat ones. We also like to add that we performed similar calculations with another flat halo profile namely Burkert profile [80, 81], but the calculated γ flux is found to be even below than what is obtained for isothermal profile.

Different flavours of neutrinos from the dark matter annihilation at galactic centre are also addressed in the present work. The flux and detection of muon species of such neutrinos are calculated for the neutralino dark matter in mAMSB model. Given the masses of such dark matter candidates the energies of such neutrinos will also be in the range GeV to TeV. The location of the galactic centre with respect to earth is downwards. The high energetic muon neutrinos may produce muons by the charged current scattering off ice or water and may be detected by their Cerenkov lights. We calculate the fluxes of neutrinos of different flavours due to annihilations of dark matter when viewed in the direction of the galactic centre as also at the other two chosen positions in its neighbourhood. The results are shown for the four halo profiles considered. In order to estimate the detection yield of such neutrinos in a terrestrial neutrino observatory, we have chosen the ANTARES under sea detector and calculated the muon yield for muon neutrinos from galactic centre for all the

four halo profiles considered. The calculations of neutrinos in case of different halo profiles also exhibit similar trend as those for the calculation of γ flux.

The value of thermal average of the squared halo density, $\langle \rho^2(r) \rangle$ is generally greater than $(\langle \rho(r) \rangle)^2$ due to the influence of a probable clumpy structure of dark matter halo profile, $F_c(r)$, which is related to dark matter halo profile by,

$$\langle \rho^2(\tilde{r}) \rangle = \rho_0^2 F_{halo}^2(r) F_c(r) \quad (33)$$

The clump structure of dark matter halo gives rise to enhancement factor. In the present study of different models of galactic halo structures, we did not consider any clumpy halo of dark matter. This study is for posterity.

The WMAP allowed zone(s) for the mAMSB model for dark matter, are around (~ 1 TeV and ~ 2 TeV) which are high in mass regime like Kaluza-Klein dark matter. The future collider experiment may verify their existence.

6 Acknowledgements

The authors thank Pijushpani Bhattacharjee and Pratik Majumdar for some useful discussions.

References

- [1] K.G. Begeman, A.H. Broeils and R.H. Sanders, Mon. Not. Roy. Astron. Soc. **249**, 523 (1991).
- [2] R. Massey *et al.*, Nature **445**, 286 (2007), arXiv:astro-ph/0701594.
- [3] D.E. McLaughlin, Astrophys. J. **512**, L9 (1999).
- [4] E.L. Lokas and G.A. Mamon, Mon. Not. Roy. Astron. Soc. **343**, 401 (2003), arXiv:astro-ph/0302461.
- [5] M. Bradac, Nucl. Phys. Proc. Suppl. **194**, 17 (2009).
- [6] C.L. Bennett *et al.*, [The WMAP Collaboration], astro-ph/0302207; D.N. Spergel *et al.* [WMAP Collaboration], Astrophys. J. Suppl. **170**, 377 (2007); E. Komatsu *et al.* [WMAP Collaboration], Astrophys. J. Suppl. **180**, 330 (2009); *ibid.* [WMAP Collaboration], Astrophys. J. Suppl. **192**, 18 (2011).
- [7] G. Jungman, M. Kamionkowski and K. Griest, Phys. Rept. **267**, 195 (1996).
- [8] K. Griest and M. Kamionkowski, Phys. Rept. **333**, 167 (2000).

- [9] G. Bertone, D. Hooper and J. Silk, Phys. Rept. **405**, 279 (2005).
- [10] H. Murayama, arXiv:0704.2276 [hep-ph].
- [11] F. Aharonian *et al.*, H.E.S.S. Collaboration, Nature **439**, 695 (2006), arXiv:astro-ph/0603021.
- [12] F. Aharonian *et al.*, H.E.S.S. Collaboration, Astron. Astrophys. **503**, 817 (2009); F. Aharonian *et al.*, Astron. Astrophys. **425**, L13 (2004).
- [13] L. Randall and R. Sundrum, Nucl. Phys. B **557**, 79 (1999).
- [14] G.F. Giudice, M.A. Luty, H. Murayama and R. Rattazzi, JHEP **12**, 027 (1998); A. Pamedal and R. Rattazzi, JHEP **05**, 013 (1999); R. Rattazzi, A. Strumia and J.D. Wells, Nucl. Phys. B **576**, 3 (2000).
- [15] H.E. Haber and G.L. Kane, Phys. Rep. **117**, 75 (1985).
- [16] ATLAS Collaboration, Eur. Phys. J. **C72**, 1993 (2012); <https://cdsweb.cern.ch/record/1432200>
- [17] A. Datta, A. Kundu and A. Samanta, Phys. Rev. D **64**, 095016 (2001).
- [18] M. Ageron *et al.* (ANTARES Collaboration), Nucl. Instrum. Meth. A **656** 11 (2011) (arXiv:1104.1607 [astro-ph.IM]).
- [19] D.A. Vásquez *et al.* Phys. Rev. D **84**, 095008 (2011).
- [20] M. Cherenyakova *et al.*, Astrophys. J. **726**, 60 (2011); T. Linden *et al.* Astrophys. J. **753**, 41 (2012).
- [21] A. Baer, R. Dermíšek, S. Rajagopalan and H. Summy, JCAP **07**, 014 (2010).
- [22] T. Moroi and L. Randall, Nucl. Phys. B **570**, 455 (2000).
- [23] P. Ullio JHEP **0106** 053 (2001).
- [24] D. Majumdar, J. Phys. G **28**, 2747 (2002).
- [25] S. Dodelson, D. Hooper and P.D. Serpico, Phys. Rev. D **77**, 063512 (2008).
- [26] <http://www-glast.slac.stanford.edu/>
- [27] P.C. Serpico and D. Hooper, New J. Phys. **11**, 105010 (2009), arXiv:0902.2539 [hep-ph].
- [28] R. Allahverdi, S. Campbell and B. Dutta, Phys. Rev. D **85**, 035004 (2012), arXiv:1110.6660 [hep-ph].

- [29] Ya.B.Zeldovich, A.A.Klypin, M.Yu.Khlopov and V.M.Chechetkin, Sov.J.Nucl.Phys. **31**, 664 (1980); D.Fargion, M.Yu. Khlopov, R.V.Konoplich and R.Mignani, Phys. Rev. D **52**, 1828 (1995).
- [30] J. Edsjö and P. Gondolo, Phys. Rev. D **56**, 1879 (1997).
- [31] G. Belanger, F. Boudjema, P. Brun, A. Pukhov, S. Rosier-Lees, P. Salati and A. Semenov, Comput. Phys. Commun. **182**, 842 (2011), arXiv:1004.1092 [hep-ph].
- [32] R. Bernabei *et al.* [DAMA collaboration], Eur. Phys. J. C **56**, 333 (2008); AIP Conf. Proc. **698**, 328 (2004); Int. J. Mod. Phys. D **13**, 2127 (2004).
- [33] Z. Ahmed *et al.* [CDMS Collaboration], Phys. Rev. Lett. **103**, 141808 (2009). <http://ppd.fnal.gov/experiments/cdms/>
- [34] Z. Ahmed *et al.* [The CDMS-II Collaboration], Science **327**, 1619 (2010), arXiv:0912.3592 [astro-ph.CO].
- [35] B. Beltran [for the PICASSO collaboration], J. Phys.:Conference series **136**, 042080 (2008).
- [36] J. Angle *et al.* (Xenon Collaboration), Phys. Rev. Lett. **100**, 021303 (2008); E. Aprile and T. Doke, Rev. Mod. Phys. **82**, 2053 (2009).
- [37] E. Aprile *et al.* [XENON100 Collaboration], Phys. Rev. Lett. **105**, 131302 (2010), arXiv:1005.0380 [astro-ph.CO]; E. Aprile *et al.* [XENON100 Collaboration], Phys. Rev. Lett. **107**, 131302 (2011); E. Aprile *et al.* [XENON100 Collaboration], Astropart. Phys. **35** 573-590
- [38] E. Behnke *et al.*, Science **319**, 933 (2008).
- [39] Akerib D.S. *et al.*, Nuclear Inst. and Methods in Physics Research A704 111 (2013)
- [40] M. Boulay *et al.*, J.Phys.Conf.Ser. **136** 042081 (2008)
- [41] R. Lemrani, EDELWEISS Collaboration, Phys. Atom. Nucl. **69**, 1967 (2006).
- [42] D.S. Akerib *et al.*, Nucl. Instrum. Meth. A **559**, 411 (2006).
- [43] T. Sumner, UKDMC Collaboration PoS **HEP2005**, 003 (2006).
- [44] V.N. Lebedenko *et al.*, Phys. Rev. D **80**, 052010 (2009), arXiv:0812.1150 [astro-ph].

- [45] H.S. Lee *et al.* [KIMS Collaboration], Phys. Rev. Lett. **99**, 091301 (2007) [arXiv:0704.0423]; S. C. KIM *et al.* [KIMS Collaboration] Phys. Rev. Lett. **108** 181301 (2012); H. S. Lee *et al.* [KIMS Collaboration] Phys. Lett. B **633** 201 (2006).
- [46] C.E. Aalseth *et al.* [CoGeNT collaboration], Phys. Rev. Lett. **106**, 131301 (2011).
- [47] G.J. Alner *et al.* [UKDMC], Phys. Lett. B **616**, 17 (2005).
- [48] T. Morlat *et al.*, arXiv:0704.2037 [astro-ph].
- [49] A. Takeda *et al.* Phys. Lett. B **572**, 145 (2003); Y. Shimizu, Phys. Lett. B **633**, 195 (2006).
- [50] T. Falk, A. Ferstl, and K. A. Olive, Astropart. Phys. **13**, 301-316 (2000), arXiv:hep-ph/9908311.
- [51] <http://cedar.berkeley.edu/plotter/entryform.html>.
- [52] O. Adriani *et al.* [PAMELA collaboration], Nature **458**, 607 (2009); O. Adriani *et al.*, Phys. Rev. Lett. **102**, 051101 (2009).
- [53] J.J. Beatty, *et al.*, Phys. Rev. Lett. **93**, 241102 (2004), arXiv:astro-ph/0412230.
- [54] M. Aguilar, *et al.*, AMS-01 Collaboration, Phys. Lett. B **646**, 145 (2007), arXiv:astro-ph/0703154.
- [55] A.A. Abdo, *et al.*, The Fermi LAT Collaboration, Phys.Rev.Lett. **102**, 181101 (2009), arXiv:0905.0025 [astro-ph.HE].
- [56] J. Chang *et al.*, Nature **456**, 362 (2008).
- [57] A.W. Strong *et al.*, Astron. Astrophys. **444**, 495 (2005), arXiv:astro-ph/0509290.
- [58] D.J. Thompson, Rept. Prog. Phys. **71**, 116901 (2008), arXiv:0811.0738 [astro-ph].
- [59] C. Meurer and FermiLAT collaboration, AIP Conf. Proc. **719**, 1085 (2009).
- [60] J. Albert *et al.* [MAGIC Collaboration], Astrophys. J. **638**, L101 (2006).
- [61] G. Maier [VERITAS Collaboration], AIP Conf. Proc. **1085**, 187 (2009).
- [62] K. Tsuchiya *et al.* [CANGAROO-II Collaboration], Astrophys. J. **606**, L115 (2004), arXiv:astro-ph/0403592.

- [63] V. Vitale *et al.* [Fermi/LAT Collaboration], arXiv:0912.3828 [astro-ph.HE].
- [64] F. Acero *et al.*, MNRAS **402**, 1877 (2010), arXiv:0911.1912 [astro-ph]..
- [65] F. Stoehr *et al.*, MNRAS **345**, 1313 (2003), arXiv:astro-ph/0307026.
- [66] D. Meritt, arXiv:1001.3706 [astro-ph.CO].
- [67] K. Kosack *et al.*, Astropart. Phys. **608**, L97 (2004).
- [68] J. Navarro, C. Frenk, S. White, Astrophys. J. **490** 493 (1997).
- [69] J. N. Bahcall and R. M. Soneira, Astrophys. J. Suppl. **44** 73 (1980).
- [70] J. Diemand, B. Moore and J. Stadel, Mon. Not. Roy. Astron. Soc. **353** 624 (2004); B. Moore *et al.*, Astrophys. J. **499** L5 (1998).
- [71] J. Einasto, Trudy Inst. Astroz. Alma-Ata **51** 87 (1965).
- [72] F. Prada, A. Klypin, J. Flix, M. Martínez and E. Simonneau, Phys. Rev. Lett. **93**, 241301 (2004).
- [73] Y. Mambrini, C. Munoz, E. Nezri and F. Prada, JCAP **0601**, 010 (2006), arXiv:hep-ph/0506204.
- [74] <http://icecube.wisc.edu>
- [75] <http://baikalweb.jinr.ru/>
- [76] <http://www.nestor.noa.gr/>
- [77] T. Schwetz, M. Tortola and J.W.F. Valle, New J. Phys. **13**, 109401 (2011), arXiv:1108.1376 [hep-ph]; M.C. Gonzalez-Garcia, M. Maltoni and J. Salvado, JHEP **1004**, 056 (2010), arXiv:1001.4524v3 [hep-ph]; G.L. Fogli, E. Lisi, A. Marrone, A. Palazzo and A.M. Rotunno, arXiv:1106.6028 [hep-ph].
- [78] J.K. Ahn *et al.*, arXiv:1204.0626 [hep-ex].
- [79] <http://www.hawc-observatory.org/>
- [80] A. Burkert, Astrophys. J. **447**, L25 (1995).
- [81] G. Gentile, B. Famaey, H. Zhao and P. Salucci, Nature **461**, 627 (2009).